Available online at www.sciencedirect.com
SCIENCE DIRECT®
Polymer 44 (2003) 4171–4177
polymer
www.elsevier.com/locate/polymer

Surface segregation of chain ends in α,ω-fluoroalkyl-terminated polystyrenes films

Keiji Tanaka[a], Daisuke Kawaguchi[a], Yasuyuki Yokoe[a], Tisato Kajiyama[a,*], Atsushi Takahara[b], Seiji Tasaki[c]

[a]*Department of Applied Chemistry, Faculty of Engineering, Kyushu University, Fukuoka 812-8581, Japan*
[b]*Institute for Materials Chemistry and Engineering, Kyushu University, Fukuoka 812-8581, Japan*
[c]*Research Reactor Institute, Kyoto University, Osaka 590-0494, Japan*

Received 6 January 2003; received in revised form 17 April 2003; accepted 12 May 2003

Abstract

α,ω-Fluoroalkyl-terminated polystyrenes (α,ω-PS(R_f)$_2$) with various molecular weights were synthesized by an anionic polymerization. Then, chain end distribution in the surface region of the α,ω-PS(R_f)$_2$ films was studied by angular-dependent X-ray photoelectron spectroscopy in conjunction with neutron reflectivity. The α,ω-PS(R_f)$_2$ films annealed under vacuum exhibited surface localization of chain ends. Since the fluoroalkyl chain ends possess a lower surface free energy compared with the main chain part, they energetically prefer to partition to the surface. The extent to which the chain ends were segregated at the surface was examined as a function of molecular weight. Also, it was presented how surface orientation of the fluoroalkyl end groups was dependent on molecular weight. On the other hand, no segregation of the chain ends was observed at the surface of the α,ω-PS(R_f)$_2$ film annealed in boiled water. This is because the chain ends with a lower surface free energy tend to stay away from the higher energy medium of the boiled water. This result reveals that the surface concentration of chain ends can be regulated by selecting an appropriate annealing condition based on surface thermodynamics.

Keywords: Surface segregation; Chain end group; Polystyrene

1. Introduction

Polymer surfaces play important and crucial roles in many technological applications [1,2]. For instance, it has been widely accepted that the wetting properties of polymeric materials are governed by physico-chemical nature of a few atomic layers at the outermost surface [3,4]. This means that if only the surface region can be precisely controlled, the wetting characteristics would be perfectly regulated without changing any bulk properties. Also, multilayer structure, e.g. gas-barrier films, thin polarizers and electro-luminescence devices, might be the case as a typical modern example of importance of polymer surfaces. Such multilayers are generally composed of different ultrathin layers, and each elemental layer possesses an extremely large surface to volume ratio. Hence, in reality, it has turned out to be necessary to design and construct these functional materials by taking into account surface and interfacial features.

Underpinning the situation mentioned above, surface aggregation states and physico-chemical properties have been intensively studied over the world thus far. Many responsible factors on surface structure and properties have been pointed out. Of such factors, chain end chemistry is quite intriguing because it drastically alters surface nature by a trivial amount [5–16]. Sometimes, it can change even bulk nature as well [17,18]. Nevertheless, the importance of chain end chemistry seems to be not necessarily recognized.

In this study, we focus on chain end distribution and orientation in the surface region of monodisperse polystyrene (PS) terminated by fluoroalkyl end groups. Since the end groups have a smaller surface free energy than that of the main chain part, it can be predicted that the both ends are preferentially segregated at the air/polymer interface. When the films are annealed under water vapor condition, how do the end groups distribute in the surface region? Also, what will happen if the films are kept in boiled

* Corresponding author. Tel.: +81-92-642-3558; fax: +81-92-651-5606.
E-mail address: kajiyama@cstf.kyushu-u.ac.jp (T. Kajiyama).

0032-3861/03/$ - see front matter © 2003 Elsevier Science Ltd. All rights reserved.
doi:10.1016/S0032-3861(03)00391-4

water for a while? Answers to these questions are derived by X-ray photoelectron spectroscopy (XPS) in conjunction with neutron reflectivity (NR).

2. Experimental section

2.1. Materials and film preparation

α,ω-(Tridecafluoro-1,1,2,2-tetrahydrooctyl)dimethylsilyl-terminated PS (α,ω-PS(R_f)$_2$) with various molecular weights were synthesized by a sequential anionic polymerization using an alkali-metal naphthylide initiator in tetrahydrofuran (THF) under argon atmosphere at 190 K. Fig. 1 shows the synthetic route of the α,ω-PS(R_f)$_2$. Styrene (St) was dried over CaH_2 for 24 h and distilled twice under vacuum. The purified monomer was stored under argon atmosphere. THF was distilled after refluxing 24 h over sodium and benzophenone under nitrogen atmosphere. Alkali-metal naphthylides (Na and K) used as bifunctional radical-ionic initiators were synthesized by the stoichiometric reaction of naphthalene with metal in THF at room temperature, and were used for the polymerization right away. (Tridecafluoro-1,1,2,2-tetrahydrooctyl)dimethylchlorosilane was used as just received. At first, THF and St were transferred into a glass reactor by a capillary technique. Then, the reactor was cooled to 190 K, and the calculated amount of the bifunctional initiator was added to the well-stirred THF solution by a syringe. After the polymerization reaction for 10 min at 190 K, the three- to fivefold excess amount of (tridecafluoro-1,1,2,2-tetrahydrooctyl)dimethylchlorosilane was added to the reactor. The product was precipitated twice into methanol and then vacuum-dried. For NR measurement, polymers (**2**; α,ω-P(dSt-*b*-St-*b*-dSt)(R_f)$_2$ and **3**; α,ω-P(dSt-*b*-St-*b*-dSt)(H)$_2$) were also synthesized by the similar procedure, but the main chain part of the both were composed of St and deuterated St units, as shown in Fig. 1. The polymer **3** was terminated by purified methanol instead of (tridecafluoro-1,1,2,2-tetrahydrooctyl)dimethyl-chlorosilane.

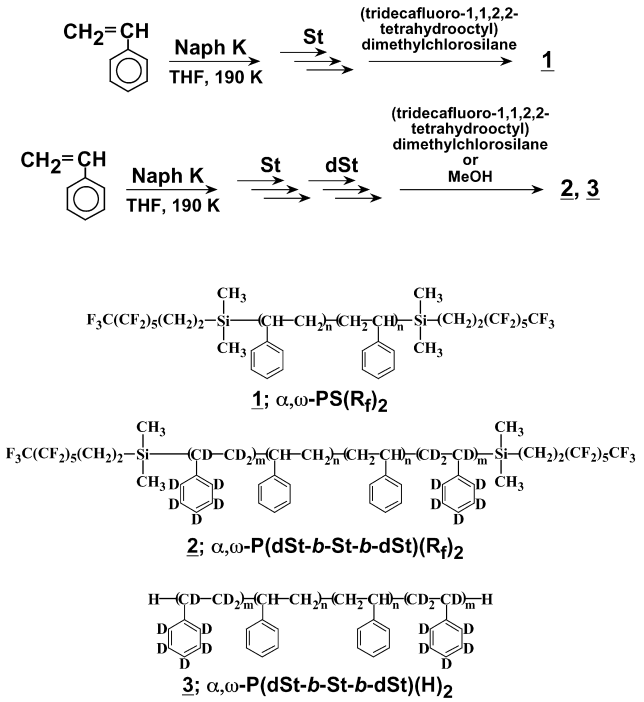

Fig. 1. Synthetic route of polymers used in this study and their chemical structures.

Polymer films were spun-coated from toluene solutions onto cleaned silicon wafers with native oxide layer, and then, dried at room temperature for more than 24 h under ambient atmosphere. The successive annealing was made at 423 K for, at least, 48 h under vacuum or water vapor, or in distilled water. Each film thickness evaluated by ellipsometric measurement was approximately, 200 nm unless the thickness was stated.

2.2. Characterizations of polymers

Number-average molecular weight, M_n, and molecular weight distribution, M_w/M_n, of the polymers obtained, where M_w denotes weight-average molecular weight, were determined by gel permeation chromatography (GPC) with PS standard. Functionality of the fluoroalkylsilane end groups was determined by nuclear magnetic resonance spectroscopy. Table 1 shows M_n, M_w/M_n, and functionality of the polymers synthesized.

Concentration profile of chain end groups in the surface region was examined by XPS in conjunction with NR. XPS (PHI 5800 ESCA system, Physical Electronics, Co., Ltd) measurement was carried out with a monochromatized Al Kα source at 14 kV and 24 mA. The main chamber of XPS was maintained at $\sim 10^{-8}$ Pa or even better. C_{1s} peak corresponding to neutral carbon was assigned to a binding energy of 285.0 eV to correct for the charging energy shift. The analytical depth of XPS, d, from the outermost surface is defined by

$$d = 3\lambda \sin\theta \quad (1)$$

where λ and θ are inelastic mean-free path of photoelectrons in a solid and emission angle of photoelectrons, respectively [19]. The inelastic mean-free path of photoelectrons was calculated by Ashley's equation [20]. The emission angle of

Table 1
Characterizations of polymers used in this study

Sample	M_n [a]	M_w/M_n [a]	Functionality [b]	$2R_g$ (nm)
α,ω-PS(R_f)$_2$	10.2k	1.09	2.0	5.3
	25.2k	1.12	1.6	8.3
	47.8k	1.18	1.5	11.8
	93.4k	1.17	1.7	16.6
α,ω-P(dSt-*b*-St-*b*-dSt)(R_f)$_2$	26.7k	1.09	2.0	8.5
α,ω-P(dSt-*b*-St-*b*-dSt)(H)$_2$	26.0k	1.11	–	8.5

[a] By GPC.
[b] By ^{1}H NMR.

photoelectrons was varied from 15° to 90° in this experiment.

NR measurement was made by the multilayer interferometer for neutrons (C3-1-2, MINE) at the Institute for Solid State Physics, the University of Tokyo. Incident neutrons have the long wavelength of 1.26 nm and the resolution of 5.1%. Reflectivity was calculated on the basis of the scattering length density profile along the depth direction using Spreadsheet Environmental Reflectivity Fitting [21].

3. Results and discussion

3.1. Surface distribution of chain ends in films annealed under vacuum

To examine the concentration profile of fluoroalkyl end groups in the surface region, XPS measurement was made at first. Fig. 2 shows typical XPS F_{1s} and C_{1s} spectra of the α,ω-PS$(R_f)_2$ film with M_n of 93.4k, collected at θ of 90°. Also, the curve 2 of the part (b) is for the α,ω-PS$(R_f)_2$ film with M_n of 10.2k at θ of 15°. The F_{1s} spectrum, which came from the chain end portion, was quite simple, whereas two peaks were apparently observed for the C_{1s} spectrum. The peak at the binding energy of 285 eV was assigned to neutral carbon, and the one at 291.5 eV was actually composed of two origins from aromatic $\pi-\pi^*$ transition and

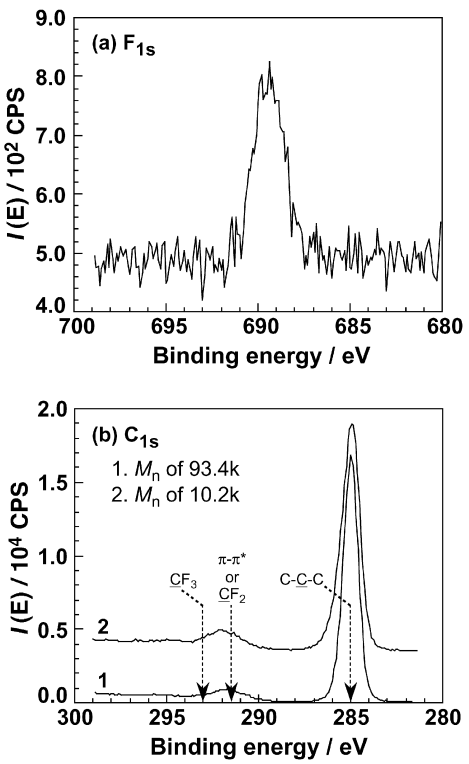

Fig. 2. Typical XPS (a) F_{1s} and (b) C_{1s} spectra for α,ω-PS$(R_f)_2$ with M_n of 93.4k, collected at θ of 90°. Curve 2 of the part (b) is for the α,ω-PS$(R_f)_2$ film with M_n of 10.2k at θ of 15°.

CF_2 carbon. The C_{1s} signal from CF_3 carbons at the binding energy of 293 eV was quite weak. When the α,ω-PS$(R_f)_2$ film with a smaller M_n was examined, the complicated peak at 291.5 eV became larger. This is because the surface concentration of the fluoroalkyl chain ends increased, resulting in an increase in the C_{1s} signal from CF_2 carbons. Since the contribution from the CF_2 carbons could be hardly dissolved from the $\pi-\pi^*$ satellite peak due to the same binding energy, the peak intensity ratio of F_{1s} to C_{1s} was used to discuss about chain end distribution near the surface, rather than peak deconvolution of the C_{1s} spectrum.

Fig. 3 shows the analytical depth dependence of peak intensity ratio of F_{1s} to C_{1s}, $I_{F_{1s}}/I_{C_{1s}}$, for the α,ω-PS$(R_f)_2$ films as a function of M_n. The films were annealed under vacuum at 423 K for 24 h. The abscissa is expressed in terms of sin θ as an index of the analytical depth. Bulk values of $I_{F_{1s}}/I_{C_{1s}}$ marked by broken lines in Fig. 3 were stoichiometrically calculated on the basis of each M_n and functionality after taking into account the atomic sensitive factors of F_{1s} and C_{1s}. For all the α,ω-PS$(R_f)_2$ films employed, $I_{F_{1s}}/I_{C_{1s}}$ value was higher than the corresponding bulk value, and became larger with decreasing sin θ. This result makes it clear that the fluoroalkyl chain ends were preferentially segregated in the surface region, and that the inclination became more remarkable closer to the surface. Although, $3\lambda \sin\theta$ corresponds well to the analytical depth as given in Eq. (1), Fig. 3 cannot be simply converted to the depth profile of F atoms, that is, chain end distribution near the surface.

In general, the photoelectrons cannot travel for a long distance in a solid due to the inelastic scattering. This means that only photoelectrons emitted from the region in close proximity to the surface can get out of the solid, resulting in the surface sensitivity of XPS technique. The intensity of photoelectrons emitted from atoms at the depth of x is defined as

$$I(\theta, x) = Fk \exp\left(-\frac{x}{\lambda \sin\theta}\right) N(x) \tag{2}$$

where F, k and $N(x)$ are transmission function, factor including capture cross-section and emission efficiency, and number of atoms at x, respectively, provided that the X-ray attenuation in the surface layer is negligible. Hence, even though the sampling depth is x, photoelectrons are not uniformly emitted from the depth region from the surface to x. Instead, the detected amount of photoelectrons exponentially decays with increasing depth to x.

Actually, several strategies have been reported to extract the real depth profile of a component from the angular-dependent XPS results [22–25]. Of such ways, we chose an easily accessible method based on Paynter's algorithm [22]. In this method, the surface region is first divided into compositionally uniform parallel layers. Since the intensity of photoelectrons from the multilayer can be given by Eq. (3), the real depth profile of the component is supposed

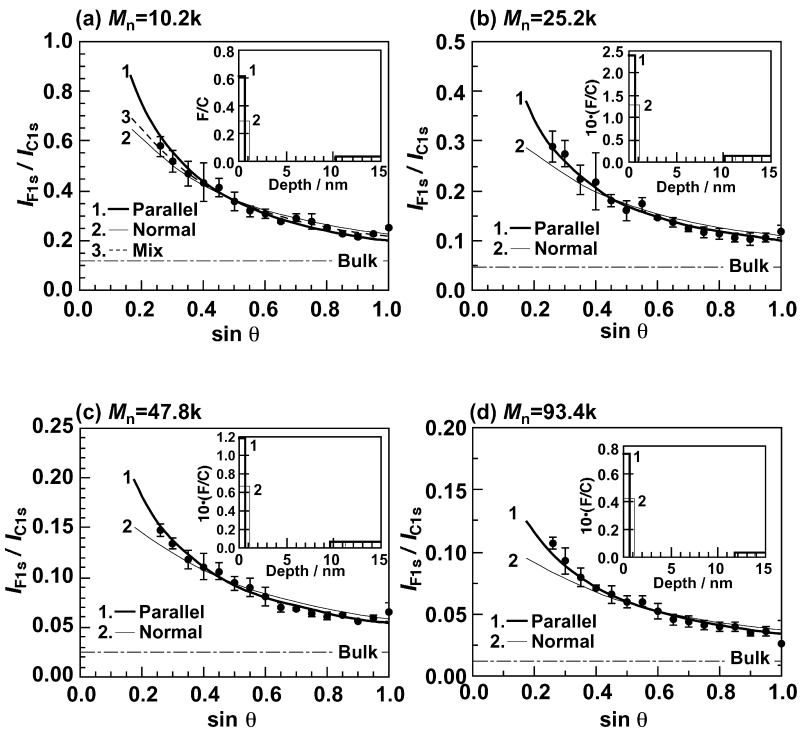

Fig. 3. Analytical depth dependence of peak intensity ratio of F_{1s} to C_{1s} for the α,ω-PS(R_f)$_2$ film as a function of molecular weight. The insets show the model depth profiles of atomic ratio of fluorine to carbon to obtain the best-fit $I_{F_{1s}}/I_{C_{1s}}$ curve assuming on parallel and normal models. The line thickness in the insets corresponds to that in the main panels.

to be deduced

$$I(\theta,x) = Fk\left(\int_0^{x_1} \exp\left(-\frac{x}{\lambda \sin\theta}\right) n_1 \, dx + \int_{x_1}^{x_2} \exp\left(-\frac{x}{\lambda \sin\theta}\right) n_2 \, dx + \cdots\right) \quad (3)$$

where n_i is the number density of atoms in a homogeneous layer from x_i to x_{i+1}. We now consider four models of the chain ends near the surface, as shown in Fig. 4. Parts (a) and (b) show situations where the chain ends are perfectly parallel and normal to the surface, respectively. In the case of the parallel model, F atoms are located in the surface region of 0.58 nm corresponding to an approximate diameter of a fluoroalkyl group. On the other hand, F atoms are partitioned to the surface region of 1.2 nm, if the chain ends are normal to the surface. This value is the length of a fluoroalkyl tail. And, mixed model in part (c) and tilt model in part (d), which might be closer to reality rather than the simple two models of (a) and (b), are also plausible.

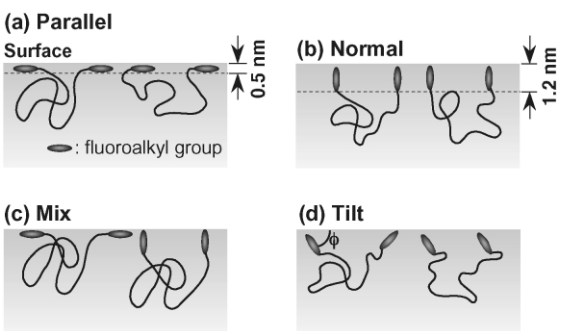

Fig. 4. Schematic representations of surface orientation for chain ends; (a) parallel, (b) normal, (c) mix, and (d) tilt.

The bold and thin solid curves in the main panels of Fig. 3 show the best-fit relation of $I_{F_{1s}}/I_{C_{1s}}$ to sin θ using the parallel and normal models, respectively. Each inset of Fig. 3 shows the model depth profile of the atomic ratio of fluorine to carbon to obtain the best-fit $I_{F_{1s}}/I_{C_{1s}}$ vs. sin θ curve, where the bold and thin lines possess the same meaning as the main panel. The fitting procedure was made under an assumption that the chain end portions were perfectly localized in the outermost layer of 0.58 nm for the parallel model or 1.2 nm for the normal one. Also, the mass balance of the chain ends through the film was strictly taken into account as follows. The total amount of the fluoroalkyl chain ends must be kept through the film even though a part of them is preferentially partitioned to the surface. Given the surface segregation layer of the chain end groups, there should exist the depletion layer of the chain ends beneath it. Beyond the depletion layer, the bulk (F/C) value was recovered, as shown in the insets. In the case of $M_n = 10.2$k, the simple normal and parallel models could not well fit the experimental result. And, the experimental $I_{F_{1s}}/I_{C_{1s}}$ was intermediate between the values deduced by the two models. Hence, the mix model was applied, and could well reproduce the experimental result with the normal and parallel

fractions of 68 and 32%, respectively, as shown in Fig. 3(a). This means that the fluoroalkyl chain ends at the surface of the α,ω-PS(R_f)$_2$ film with M_n = 10.2k mostly exist along the normal direction. Also, the tilt model with the ϕ of 63° could reproduce the experimental result as well (not shown). In contrast, the sin θ–$I_{F_{1s}}/I_{C_{1s}}$ curves for the α,ω-PS(R_f)$_2$ films with M_n = 25.2k, 47.8k and 93.4k were almost the same as those calculated on the basis of the parallel model. That is, the end groups for shorter α,ω-PS(R_f)$_2$ chains tend to orient normal to the surface, whereas in the case of longer α,ω-PS(R_f)$_2$ chains, the end groups prefer to sit on the surface. Hence, it is conceivable that the surface orientation of the fluoroalkyl chain ends is dependent on its chain length.

The surface localization of the fluoroalkyl end groups is driven by its lower surface free energy than the main chain part. In that sense, the parallel orientation of the end groups is favorable to minimize the free energy of the system because the number density of fluorine atoms at the outermost surface becomes higher. However, this was not the case for the α,ω-PS(R_f)$_2$ film with M_n = 10.2k, probably due to the restricted internal freedom related to probable conformation. In comparison with achieving the normal orientation, a chain suffers from less conformational entropy so that the chain ends orient parallel to the surface. This is crucial for a shorter chain. With increasing chain length, the internal freedom increases and thus the aforementioned entropic suffering would become negligible. As a result, the enthalpic factor dominates over the entropic one, resulting in the parallel orientation of the chain ends at the α,ω-PS(R_f)$_2$ film surface with a higher M_n.

Postulating that the model (F/C) vs. depth relation for the best-fitting reflects the chain end distribution near the surface, the following discussion would be possible. The surface (F/C) value was higher than the corresponding bulk one by almost 20 times. Then, the surface physical properties would vary with M_n. We now surmise by the surface localization of the chain ends of how much glass transition temperature, T_g, at the surface decreases. Fig. 5 shows M_n dependence of T_g depression at the surface, which was calculated on the basis of Fox–Flory equation [17]

$$T_g = T_{g,\infty} - K_M/M_n \quad (4)$$

where $T_{g,\infty}$ is the T_g for a chain with the infinite M_n, and K_M is a material constant. Here, $T_{g,\infty}$ of 380 K and K_M of 1.7×10^5 were used as typical numbers for PS [17]. At a higher M_n region, T_g depression at the surface is trivial because the absolute number density of the chain ends is small. However, once M_n falls short of 10^6, the chain end effect on the surface T_g depression starts to appear, as shown in Fig. 5. For example, at M_n of 10^5, the T_g depression can be claimed to be roughly −30 K. Although the manifestation mechanism of the peculiar T_g depression at the surface is not so simple in reality [26], the discussion made here is qualitatively in accordance with what has been observed so far [6].

To strengthen our simple model analysis for the angular-dependent XPS results, specular NR measurement was carried out. Here, α,ω-P(dSt-*b*-St-*b*-dSt)(R_f)$_2$ with the dSt fraction of 29 mol% was used as a sample instead of the α,ω-PS(R_f)$_2$. Since the scattering length density, (*b*/*V*), of the dSt block is much larger than that of the St block, the distribution of the chain end portions connected to the dSt block can be studied [7d]. Part (a) of Fig. 6 shows the

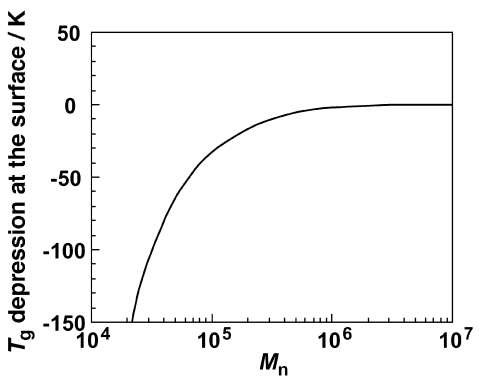

Fig. 5. Calculated T_g depression at the surface by chain end segregation as a function of M_n. The calculation was made on the basis of Fox–Flory equation with constants for PS.

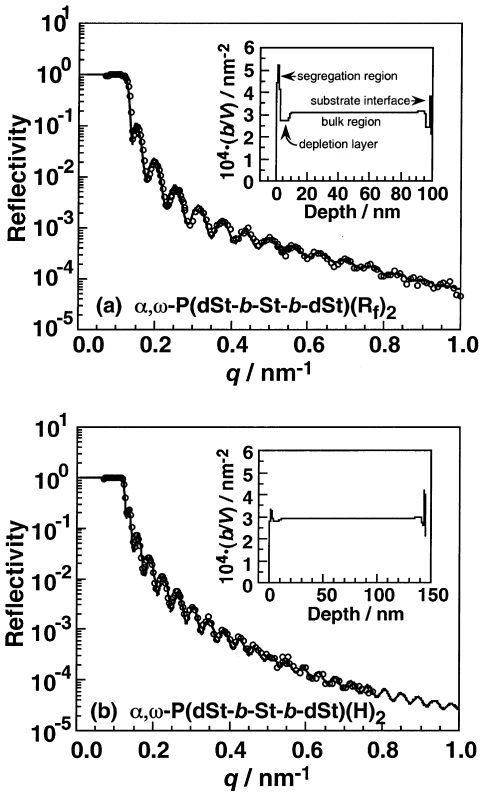

Fig. 6. Neutron reflectivity profiles for α,ω-P(dSt-*b*-St-*b*-dSt)(R_f)$_2$ with M_n of 26.7k and α,ω-P(dSt-*b*-St-*b*-dSt)(H)$_2$ with M_n of 26.0k films. Each inset shows the model scattering length density profile normal to the surface to obtain the best-fit calculated reflectivity.

scattering vector, q, dependence of NR for the α,ω-P(dSt-*b*-St-*b*-dSt)$(R_f)_2$ film with M_n of 26.7k. Here, q is given by $(4\pi/\lambda_N)\sin\theta_N$, where λ_N and θ_N are neutron wavelength and incident angle, respectively. Also, the film thickness for the NR measurement was changed to be thinner such as 94 nm. This makes the following fitting procedure easier by virtue of the appearance of Kiessig fringe. The solid line denotes the best-fit calculated reflectivity to the experimental data based on the model scattering length density, (b/V), profile shown in the inset. Since the calculated curve was in good accordance with the experimental data, it seems most likely that the model (b/V) profile corresponds well to the composition profile in the film along normal to the surface. Actually, the surface region of the model (b/V) profile down to 15 nm was constructed on the basis of the XPS model for the α,ω-PS$(R_f)_2$ with M_n of 25.2k, as shown in the inset of Fig. 3(b). Then, keeping the mass balance of the dSt component through the film, the (b/V) profile near the interface with the substrate was varied to obtain the best-fit reflectivity curve. At the surface, the (b/V) value was much higher than that in the interior region, meaning that the chain ends were preferentially segregated at the surface. And, the depletion layer related to the chain ends was also present beneath the segregation layer, as shown in the inset of Fig. 6(a). The (b/V) value of approximately $4 \times 10^{-4}\,\mathrm{nm}^{-2}$ located at the depth of about 98 nm corresponds to native oxide layer of the silicon wafer. The (b/V) value on the polymer/substrate interface was lower than that in the bulk region. Thus, it is apparent that the chain ends existed less at the interface, in contrast to the surface region. Since the native oxide layer is hydrophilic, the hydrophobic chain ends would energetically prefer to stay away from the substrate. This is what was observed at the interface. Essentially, NR measurement revealed the validity of our XPS analysis and, in addition, the interfacial distribution of the chain ends.

So far we have examined the surface and interfacial distributions of the chain ends using the α,ω-PS$(R_f)_2$ and the α,ω-P(dSt-*b*-St-*b*-dSt)$(R_f)_2$. The fluoroalkyl end groups possess an extremely lower surface free energy, which is mainly governed by energetic contribution rather than entropic origin, meaning that the chain end segregation at the surface is mainly motivated by the energetic factor. To examine what would happen if both the chain ends were replaced by repeating units terminated by proton, NR measurement was made using α,ω-P(dSt-*b*-St-*b*-dSt)$(H)_2$. Fig. 6(b) shows the q vs. reflectivity relation for the α,ω-P(dSt-*b*-St-*b*-dSt)$(H)_2$ film with M_n of 26.0k. The solid reflectivity denotes the best-fit curve calculated from the inset. A similar distribution of the chain ends was seen at the surface and the substrate interface as well, although their extents were different from those for the α,ω-P(dSt-*b*-St-*b*-dSt)$(R_f)_2$ film. In general, a chain end portion has a larger freedom compared with the main chain part, that is, it would have a larger entropic force. Therefore, the surface free energy of the chain end groups is supposed to be smaller than that of the main chain part, even though an enthalpic contribution is trivial. This is the reason why the chain ends were also segregated and depleted at the surface and interface, respectively, for the α,ω-P(dSt-*b*-St-*b*-dSt)$(H)_2$ film. Also, it has been revealed that in the case of PS with both end groups of *sec*-butyl group, α,ω-PS(*sec*-Bu), the surface segregation became more remarkable than that of PS both terminated protons which was chemically the same as the α,ω-P(dSt-*b*-St-*b*-dSt)$(H)_2$ [27].

3.2. Surface distribution of chain ends in films annealed hydrophilic conditions

We now turn to the chain end distribution in the films annealed under hydrophilic environments. As the α,ω-PS$(R_f)_2$ film annealed under water vapor, the sample was first annealed under vacuum at 423 K for 24 h, and then, kept in a glass chamber for exposure to water vapor at 373 K for 24 h. Also, for annealing in boiled water, the α,ω-PS$(R_f)_2$ film pre-annealed under vacuum was kept in a pressure-proof glass bottle filled by boiled water at 373 K. During this treatment, water was bubbled by argon gas with the purity of 99.999% to avoid the surface oxidation of the film. After sufficient drying, XPS measurement for the both films was carried out. Fig. 7 shows the sin θ dependence of $I_{F_{1s}}/I_{C_{1s}}$ for the α,ω-PS$(R_f)_2$ films with M_n of 25.2k. For comparison, the data for the vacuum-annealed film were also plotted in it as open small circles. In the case of the α,ω-PS$(R_f)_2$ film annealed under water vapor, the $I_{F_{1s}}/I_{C_{1s}}$ values, filled circles, were still higher than the stoichiometric bulk value. And also, the $I_{F_{1s}}/I_{C_{1s}}$ value increased on getting closer to the surface. This result clearly shows that the fluoroalkyl chain ends were enriched at the surface, even though the α,ω-PS$(R_f)_2$ film was annealed under water vapor. However, comparing the $I_{F_{1s}}/I_{C_{1s}}$ values between the two films at a given sin θ, it can be claimed that when the film was annealed under water vapor, the surface segregation of the chain ends was

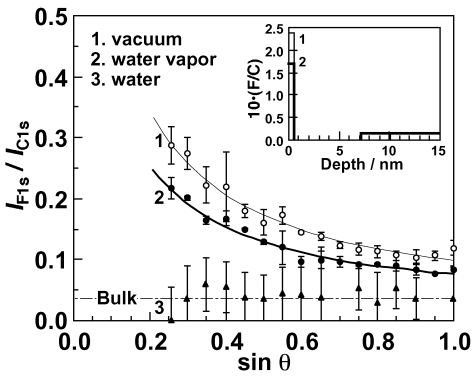

Fig. 7. Analytical depth dependence of peak intensity ratio of F_{1s} to C_{1s} for the α,ω-PS$(R_f)_2$ films annealed under vacuum and water vapor and in boiled water. The inset shows the model depth profiles of atomic ratio of fluorine to carbon to obtain the best-fit $I_{F_{1s}}/I_{C_{1s}}$ curve. The line thickness in the inset corresponds to that in the main panel.

depressed. This argument is clearly seen in the inset of Fig. 7, where the bold and thin lines correspond to the best-fit depth profiles of the chain ends for the films annealed under water vapor and vacuum. In contrast, the $I_{F_{1s}}/I_{C_{1s}}$ variation with the depth for the film annealed in boiled water was totally different in shape from those for the previous two films. The $I_{F_{1s}}/I_{C_{1s}}$ value was invariant with respect to sin θ, and almost the same as the stoichiometric bulk value, as shown in Fig. 7. Thus, it can be envisaged that the chain ends were homogeneously distributed normal to the surface, rather than the surface enrichment, for the α,ω-PS$(R_f)_2$ film annealed in boiled water. This is because the chain ends with a lower surface free energy prefer to stay away from the high surface free energy medium of boiling water. These results reveal that adopting appropriate annealing conditions based on the surface and interfacial thermodynamics can regulate the surface concentration of chain ends. In a sense, this may lead to control surface properties as well.

4. Conclusions

α,ω-PS$(R_f)_2$ with various molecular weights were synthesized by an anionic polymerization. Then, the surface aggregation states of chain ends in the α,ω-PS$(R_f)_2$ films annealed under vacuum were studied as a function of molecular weight. Model analysis of angular-dependent XPS results revealed that the surface chain end concentration was higher than the corresponding bulk value due to its lower surface free energy, and that surface orientation of chain ends was dependent on molecular weight. The conclusion made after XPS model analysis was well advocated by NR measurement. When the α,ω-PS$(R_f)_2$ film was annealed in boiled water, discernible segregation of the chain ends was not observed at the surface. This is because the chain ends with lower surface free energy prefer to stay away from the high surface free energy medium of boiling water. This result reveals that the surface concentration of chain ends can be regulated by selecting appropriate annealing conditions based on surface thermodynamics.

Acknowledgements

We are most grateful for helpful discussion with Dr Hideaki Yokoyama, AIST. This was in part supported by a Grant-in-Aid for Scientific Research (A) (#13355034) from the Ministry of Education, Culture, Sports, Science, and Technology, Japan. Also, this was partially supported by the Inter-Univ. Program for common use JAERI facility.

References

[1] Garbassi F, Morra M, Occhiello E. Polymer surfaces from physics to technology. Chichester: Wiley; 1994.
[2] Jones RAL, Richards RW. Polymers at surfaces and interfaces. Cambridge: Cambridge University Press; 1999.
[3] Schrader M, Loeb G. Modern approach to wettability: theory and applications. New York: Plenum Press; 1992.
[4] Adamson AW, Gast AP. Physical chemistry of surfaces, 6th ed. New York: Wiley; 1997.
[5] Bender GW, Gains Jr GL. Macromolecules 1970;3:128.
[6] (a) Tanaka K, Taura A, Ge SR, Takahara A, Kajiyama T. Macromolecules 1996;29:3040. (b) Kajiyama T, Tanaka K, Takahara A. Macromolecules 1997;30:280. (c) Jiang X, Tanaka K, Takahara A, Kajiyama T. Polymer 1998;39:2615. (d) Kajiyama T, Tanaka K, Takahara A. Macromolecules 1998;31:3746. (e) Tanaka K, Jiang X, Nakamura K, Takahara A, Kajiyama T, Ishizone T, Hirao A, Nakahama S. Macromolecules 1998;31:5148. (f) Satomi N, Tanaka K, Takahara A, Kajiyama T, Ishizone T, Nakahama S. Macromolecules 2001;34:8761.
[7] (a) Yilgor I, Gallagher P, Krukonis V. Macromolecules 1993;26:3069. (b) Jalbert C, Koberstein JT, Balaji R, Bhatia Q, Salvati L, Yilgor I. Macromolecules 1994;27:2409. (c) Lenk TJ, Lee DHT, Koberstein JT. Langmuir 1994;10:1857. (d) Elman JF, Johs BD, Long TE, Koberstein JT. Macromolecules 1994;27:5341. (e) Jalbert C, Koberstein JT, Hariharan A, Kumar SK. Macromolecules 1997;30:4481. (f) Koberstein JT, Duch DE, Hu W, Lenk TJ, Bhatia R, Brown HR, Lingelser JP, Gallot Y. J Adhes 1998;66:229. (g) Yuan CG, Meng OY, Koberstein JT. Macromolecules 1999;32:2329. (h) Mason R, Jalbert CA, Muisener PAVO, Koberstein JT, Elman JF, Long TE, Gunesin BZ. Adv Colloid Interface Sci 2001;94:1.
[8] (a) Frantz P, Leonhardt DC, Granick S. Macromolecules 1991;24:1868. (b) Ruths M, Granick S. J Phys Chem B 1998;102:6056. (c) Ruths M, Granick S. J Phys Chem B 1999;103:8711.
[9] Affrossman S, Hartshorne M, Jerome R, Pethrick RA, Petitjean S, Vilar MR. Macromolecules 1993;26:6251.
[10] Mayes AM. Macromolecules 1994;27:3114.
[11] Schaub TF, Kellog GJ, Mayes AM, Kulasekere R, Ankner JF, Kaiser H. Macromolecules 1996;29:3982.
[12] Henn G, Bucknall DG, Stamm M, Vanhoorne P, Jerome R. Macromolecules 1996;29:4305.
[13] Bousmina M, Qiu H, Grmela M, Klemberg-Sapieha JE. Macromolecules 1998;31:8273.
[14] Biltresse S, Descamps D, Boxus T, Marchand-Brynaert J. J Polym Phys, Part A: Polym Chem 2000;38:3510.
[15] Kumar SK, Jones RL. Adv Colloid Interface Sci 2001;94:33.
[16] (a) Sugiyama K, Hirao A, Nakahama S. Macromol Chem Phys 1996;197:3149. (b) Hirao A, Koide G, Sugiyama K. Macromolecules 2002;35:7642.
[17] Fox T, Flory P. J Polym Sci 1954;14:315.
[18] (a) Lee MH, Fleischer CA, Morales AR, Koberstein JT, Koningsveld R. Polymer 2001;42:9163. (b) Schacht PA, Koberstein JT. Polymer 2002;43:6527.
[19] Andrade JD. Surface and interfacial aspects of biomedical polymer. Surface chemistry and physics, vol. 1. New York: Plenum Press; 1985.
[20] Ashley JC. IEEE Trans Nucl Sci 1980;NS-27:1454.
[21] Welp KA, Co CC, Wool RP. J Neutron Res 1999;8:37.
[22] Paynter RW. Surf Interface Anal 1981;3:186.
[23] Yih RS, Ratner BD. J Electron Spectrosc Relat Phenom 1987;43:61.
[24] (a) Chen X, Ho T, Wynne KJ, Gardella Jr JA. Macromolecules 1995;28:1635. (b) Mahoney CM, Gardella Jr JA, Rosenfeld JC. Macromolecules 2002;35:5256.
[25] Williams JM, Beebe TP. J Vac Sci Technol, A 1997;15:2122.
[26] Tanaka K, Takahara A, Kajiyama T. Macromolecules 2000;33:7588.
[27] Tanaka K, Ariura F, Takahara A, Kajiyama T. Unpublished data.